The prestress-dependent mechanical response of magnetorheological elastomers

2015 Smart Mater. Struct. 24 085032

(http://iopscience.iop.org/0964-1726/24/8/085032)

IOP Publishing Smart Materials and Structures
Smart Mater. Struct. 24 (2015) 085032 (9pp) doi:10.1088/0964-1726/24/8/085032

The prestress-dependent mechanical response of magnetorheological elastomers

Jiabin Feng[1], Shouhu Xuan[1], Taixiang Liu[1], Lin Ge[1], Lixun Yan[2], Hong Zhou[1] and Xinglong Gong[1]

[1] CAS Key Laboratory of Mechanical Behavior and Design of Materials, Department of Modern Mechanics, University of Science and Technology of China, Hefei, 230027, People's Republic of China
[2] Department of Precision Machinery and Instrumentation, University of Science and Technology of China, Hefei 230027, People's Republic of China

E-mail: gongxl@ustc.edu.cn

Received 10 March 2015, revised 4 June 2015
Accepted for publication 15 June 2015
Published 23 July 2015

Abstract

Magnetorheological elastomers (MREs) are intelligent materials consisting of a rubber matrix filled with magnetizable particles. In many engineering applications, MREs are usually pre-confined and work with constraint-induced prestress. The prestress can significantly change the mechanical properties of MREs. In this work, the influence of prestress on the mechanical response of MREs is studieds both experimentally and theoretically. The storage modulus as well as the magneto-induced modulus change non-linearly with increasing prestress and three regions can be found in the non-linear change. In the non-full contact region, the MREs present poor mechanical properties at small prestress due to the unevenness of the sample surface. In the full contact region, the MREs are under suitable prestress, thus they present good mechanical properties. In the overload region, the pre-configured microstructure of the MREs is destroyed under the large prestress. Moreover, an analytical model is proposed to study the prestress-dependent mechanical properties of MREs. It is revealed that the prestress can change the inter-particle distance, thus further affecting the mechanical response of MREs.

Keywords: magnetorheological elastomers, prestress, microstructure, macroscopic response

(Some figures may appear in colour only in the online journal)

1. Introduction

Magnetorheological elastomers (MREs) are a class of smart materials developed by embedding micron-sized magnetic particles in a rubber or rubber-like matrix [1–3]. These composite materials can undergo large strains and exhibit excellent magnetoelastic coupling effects when stimulated by an external magnetic field [4]. The storage modulus and stiffness vary continuously with the applied magnetic field within a short time [5]. Therefore, MREs have been widely applied [6] in tunable vibration absorbers [7] and damping components [8], isolators [9–12], noise barrier systems [13], sensors [14], etc.

Because the performance of MRE devices is critically dominated by the magneto-induced properties of the MREs, a large amount of research has focused on improving the magneto-induced modulus and the relative MR effects. Various parameters for the MR effect, such as the particles [15], polymer matrix [16], anisotropic characteristics [17], interfaces [18], etc, have been systematically investigated. It was found that the microstructure of MREs has a strong impact on their macroscopic response [19–21]. To this end, the factors that could affect the inner microstructure of the MREs became the central focus of research. Moreover, prestress was found to be inevitable during the installation of MREs in engineering applications, which can change the stiffness of the MREs and the distance between particles [22–25]. When MREs are fixed to instrument surfaces, it is difficult to replace the MREs in the case of destruction. Therefore, the mechanical response of MREs under different prestress states when not adhered to instrument surfaces should be fully evaluated so as to adapt them in defined applications.

Danas *et al* [26] presented a combined experimental and theoretical study of the macroscopic response of anisotropic MREs with different initial particle chain orientations under different prestress levels and magnetic fields. A strong prestress-dependent magnetostriction was observed. Dong *et al* [27] found that the distance between the adjacent carbonyl iron (CI) particles decreased with increasing normal pressure, and eventually caused the increase of the magnetostatic force as well as the magneto-induced modulus. Liao *et al* [28] measured the magneto-induced normal force of MREs under compression. By increasing the precompression force, the magneto-induced normal force increased, which resulted from the enlargement of the interactions among the iron particles. However, normal pressure (the normal force during testing) differs from prestress (the pressure initially imposed before testing). To our knowledge, an understanding of the detailed mechanism of prestress on the mechanical properties of MREs is still lacking although several studies have been published in this area. More experimental and theoretical studies should be performed, not only for fundamental interest but also to achieve high efficiency and facility in practical applications.

In this work, both experimental and theoretical methods are employed to investigate the prestress-dependent mechanical properties of MREs. Various factors such as the particle volume fractions, magnetic fields and prestrain are considered. The optimum prestress range is obtained for different working conditions, thus this work will benefit the design of MRE devices. Moreover, an approximate model is proposed to better understand the mechanism of these mechanical responses. The calculation results agree well with the experimental analysis.

2. Experiments

2.1. Sample preparation

A group of anisotropic MREs with, respectively, 0.056, 0.118 and 0.239 CI particles by volume were fabricated. The materials consisted of CI particles (type CN, with an average diameter pf 6 μm, provided by BASF Co., Germany), HTV silicone rubber (type MVQ 110-2, provided by Dong Jue Fine Chemicals Nanjing Co., Ltd, China), dimethyl-silicon oil (acting as a plasticizer, with a viscosity of 50 cP, provided by Shanghai Resin Factory, China) and a vulcanizing agent (double methyl double benzoyl hexane, from Shenzhen Gujia Co., China).

The fabrication of anisotropic MREs consists of four major steps, as shown in figure 1(a). First, a double-roll mill (Taihu Rubber Machinery Factory, China, Model XK-160) was used to mix the CI particles, dimethyl-silicon oil and vulcanizing agent homogeneously with the silicone rubber. Second, a vacuum drying oven (Jing Hong Laboratory Instrument Co., Ltd, China, Model DZF-6050) was used to reduce the air bubbles in the rubber mixture. Third, the rubber mixture was placed into an aluminum mold. The mold was fixed to a customized magneto-heat-coupled device, which

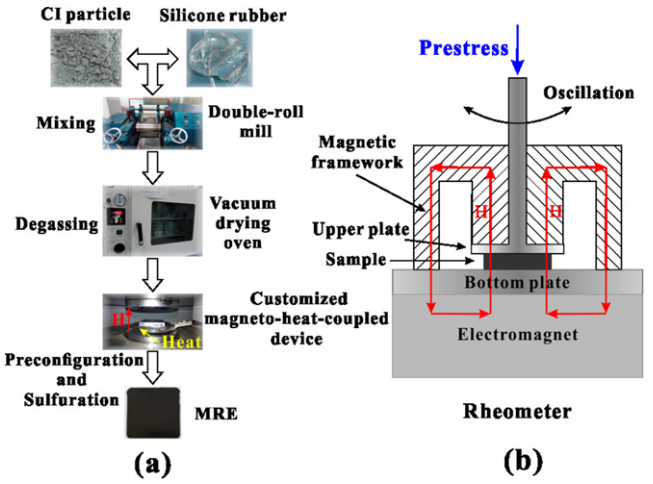

Figure 1. Schematic representations of (a) sample preparation and (b) testing.

can supply a selected magnetic field perpendicular to the mold plane and maintain the rubber mixture at a fixed temperature. In the forming pre-configuration process, the magnetic flux density was 1.5 T and the temperature was maintained at 120 °C for about 20 min Finally, during sulfuration, the magnetic flux density was maintained at 0.2 T and the temperature was increased up to 160 °C for 5 min After that, the anisotropic MRE samples were obtained.

2.2. Characterization and mechanical property testing

The microstructures of the anisotropic MREs were observed using a scanning electron microscope (SEM, Philips of Holland, Model XT30 ESEM-MP). As shown in figure 1(b), the mechanical properties of the anisotropic MREs under various prestresses were tested using a rheometer (Physica MCR 301, Anton Paar). The magnetic field perpendicular to the test plates was generated by a built-in electromagnet. The size of each sample was 10 mm in diameter and 1 mm in thickness. The sample was placed at the center of the test plate. The process of the prestress test was as follows. To begin, a selected prestress was applied to the sample and the relative position was maintained. Then, the samples were tested by varying the magnetic field strengths from 0 kA m^{-1} to 800 kA m^{-1}. During the dynamic tests, the temperature was fixed at 25 °C. Take the sample $\phi = 0.118$ as an example. Figure 2(a) demonstrates the behavior of the MREs under strain sweep from 0.005% to 5%. The storage modulus G' remains almost constant. When the shear strain exceeds 0.05%, it decreases rapidly. Figure 2(b) presents the frequency dependency of the storage modulus, which indicates that the storage modulus G' of the sample remains at a relative high level when the frequency changes from 5 Hz to 15 Hz. Therefore, during the measurements, the real strain amplitude was set at 0.05% and the frequency was 5 Hz. Each sample was tested at least three times under the same conditions.

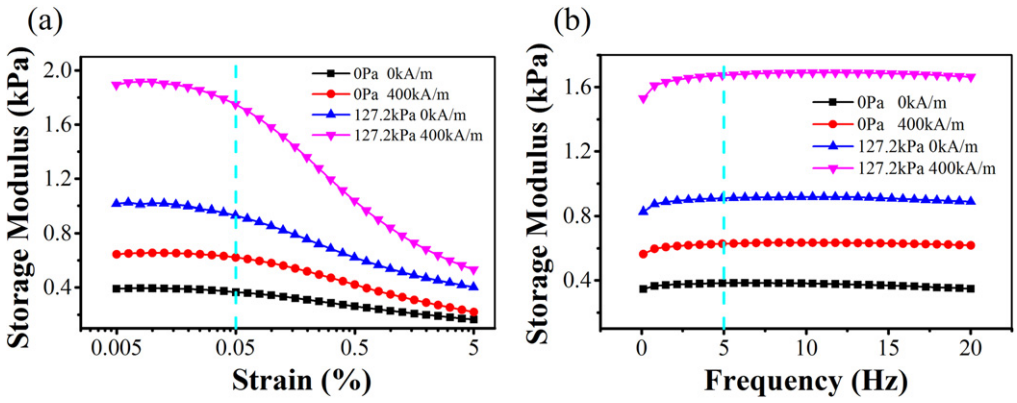

Figure 2. (a) Strain sweep test and (b) frequency sweep test of $\phi = 0.118$.

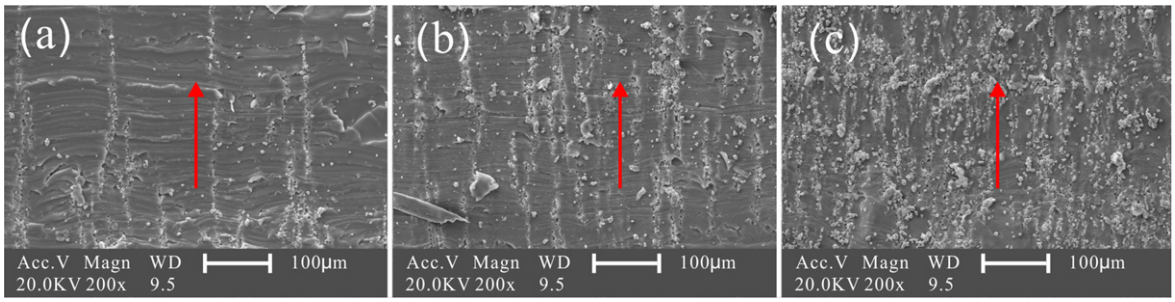

Figure 3. SEM images of the internal microstructure of the MRE samples with different particle volume fractions: (a) $\phi = 0.056$, (b) $\phi = 0.118$ and (c) $\phi = 0.239$.

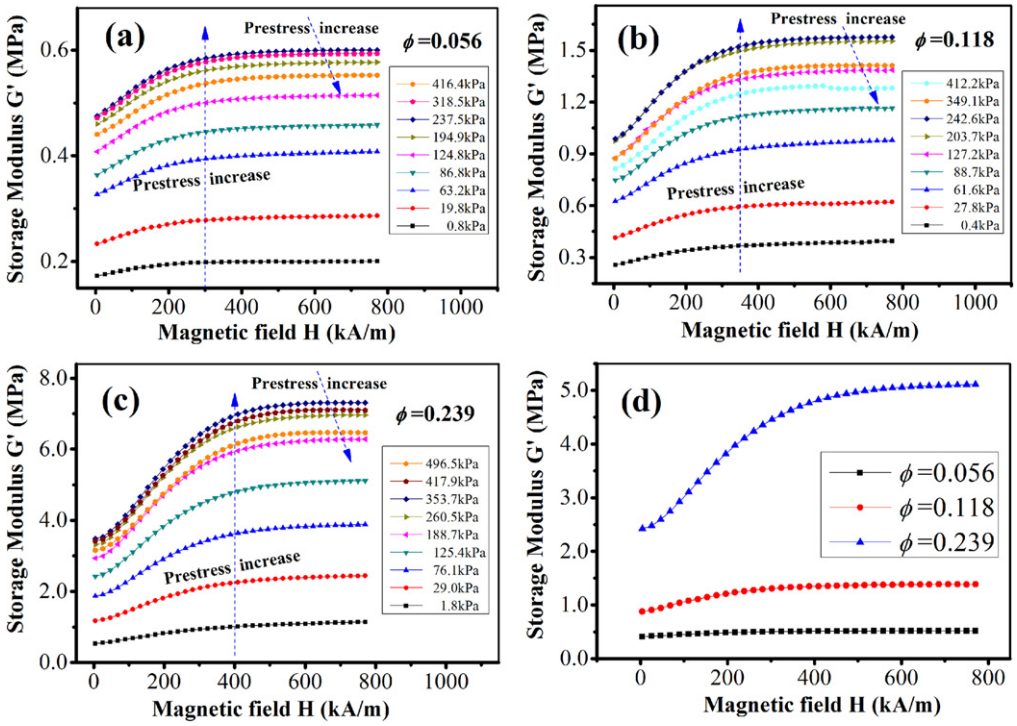

Figure 4. The storage modulus G' versus the applied magnetic field strength H for different particle volume fraction ϕ samples under various prestresses σ: (a) $\phi = 0.056$, (b) $\phi = 0.118$ and (c) $\phi = 0.239$. In (d) the prestress was roughly fixed at 125 kPa.

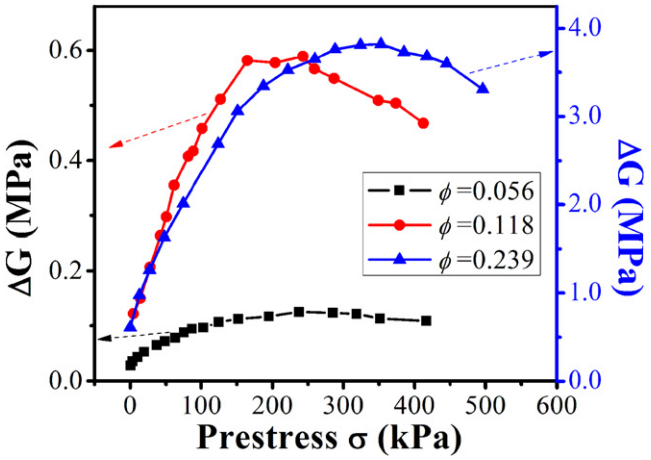

Figure 5. The magneto-induced modulus ΔG versus the applied prestress σ for different volume fraction samples.

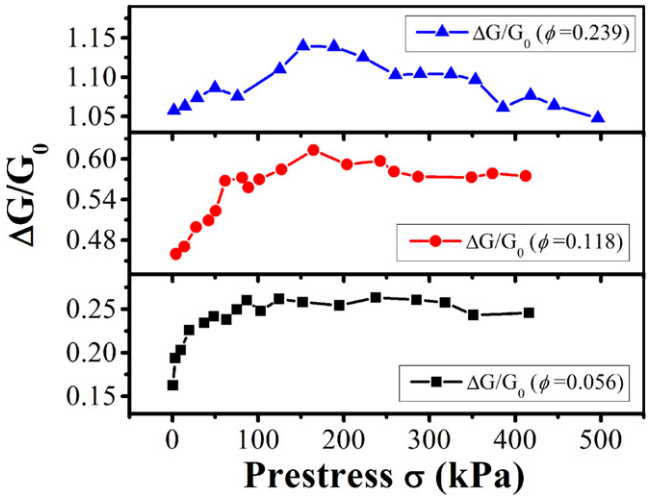

Figure 6. The relative MR effect $\Delta G/G_0$ versus the applied prestress σ for different volume fraction samples.

3. Results and discussion

Figure 3 presents typical SEM images of the as-prepared MREs. Because the MREs were prepared under a magnetic field, the CI particles assembled to form column-like structures parallel to the direction of the magnetic field. By increasing the CI content, i.e. from 0.056 to 0.118 and then to 0.239, the density of the particle chains increased and the distance between the chains decreased.

Figure 4 shows the magnetic-dependent whole storage modulus G' of the MREs under various prestresses σ. Taking the MRE with $\phi = 0.056$ as an example (figure 4(a)), at a fixed prestress, the magnitude of G' increases with increasing magnetic field strength. As soon as the magnetic field strength reaches the critical value $H = 300\,\mathrm{kA\,m^{-1}}$, G' becomes saturated. Here, the prestress plays a key role on G'. If the prestress changes from 0.8 kPa to 237.5 kPA, G' increases. However, when the prestress is higher than 237.5 kPa, G' decreases. Clearly, an optimum critical prestress can be found for each MRE sample in terms of this effect.

As shown in figures 4(b) and (c), similar results were also obtained for the MREs with CI contents of 0.118 or 0.239. However, the saturated magnetic field strengths for the three samples were different and varied from 300 to 350 and 400 $\mathrm{kA\,m^{-1}}$, respectively. Moreover, the optimum prestress also increased to 242.6 kPa and 353.7 kPa with increasing CI content. To clearly observe the influence of the CI content, the G' for different volume fractions are shown in figure 4(d), keeping the applied prestress at 125 kPa. With an increase of the CI content, both the zero storage modulus G_0 and the saturated G' of the higher content MRE are larger than those for the lower content one. For each MRE sample with a defined CI content, the applied prestress must affect the particle–particle and particle–polymer interactions, thus the whole storage modulus varies under the same magnetic field. To this end, the MRE should be fixed under a proper prestress on devices in practical applications.

The magneto-induced modulus ΔG is vital to evaluate the MREs. Figure 5 shows the ΔG of the MREs with different CI contents which change in a nonlinear way with respect to the variation of prestress. A two-step change can be distinguished for all three samples. At small prestresses, ΔG increases, while it presents a decreasing trend at large prestresses. This result also illustrates that there is an optimum prestress for each MRE sample to obtain the largest ΔG. Although the optimum prestress values for ΔG are not the same as the values for G', they show similar characteristic change and increase with CI content.

The relative MR effect, which is usually defined as $\Delta G/G_0$, was the dominant property in the practical performance. Figure 6 demonstrates the influence of the prestress on the relative MR effect. The particle volume fraction has a positive impact on the relative MR effect, which means that a higher particle volume fraction sample exhibits a larger relative MR effect. Observably, the change of the relative MR effect under different prestresses is divided into three areas. First, the relative MR effect is low at small prestresses, then increases to a high value and remains constant, and finally decreases at large prestresses.

To obtain a better understanding the effect of prestress on the mechanical response of the MREs, the MRE with $\phi = 0.118$ was chosen as a typical example to study the microscopic mechanism. As shown in figure 7, G_0 and ΔG increase with increasing prestress, then reach their largest values at a critical prestress and finally decrease at large prestresses. The prestrain versus prestress is also shown in figure 7. Interestingly, the curve begins with a nonlinear range (the Young's modulus increases with increasing prestress), goes through an approximately linear range (the Young's modulus remains almost constant) and finally ends with a nonlinear range (the Young's modulus experiences a slow decline at large prestresses).

In general, the Young's modulus of an elastomer could be regarded as an approximate constant within the scope of the elastic limit. As shown in figure 7, the ε–σ curve behaves nonlinearly at small prestresses. Based on the SEM image (figure 8 inset), it can be concluded that the small Young's

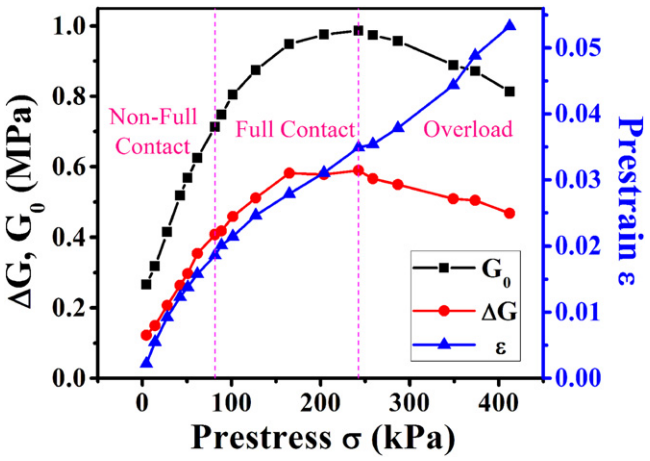

Figure 7. The zero storage modulus G_0, magneto-induced modulus ΔG and prestrain ε versus the applied prestress σ for a particle volume fraction $\phi = 0.118$.

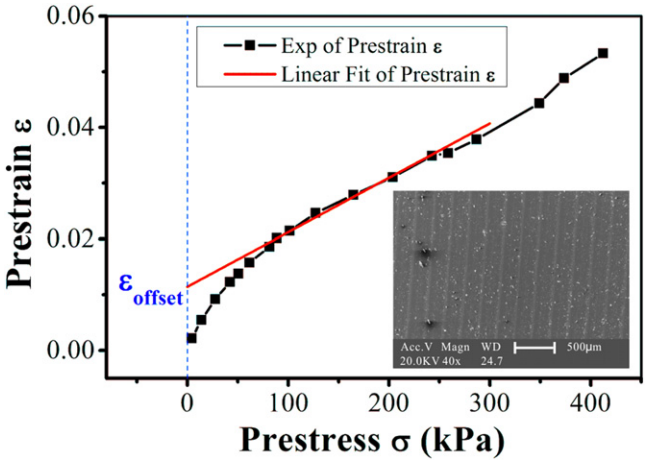

Figure 8. The prestrain ε versus the applied prestress σ for $\phi = 0.118$ and its linear fit. The inset shows an SEM image of the surface of the MRE sample.

modulus can be attributed to the uneven surface of the sample caused by the roughness of the curing mold. Furthermore, the nonlinear range of the ε–σ response and the decline of G_0 at large prestresses result from the softening of the MRE. After suffering from overload prestress, the stiffness decreases, which implies that the overload prestress may destroy the internal structure of the MRE sample.

Based on the above analysis, three regions can be observed from these experiments (figure 7). The non-full contact region refers to the region at small prestresses (smaller than 88.7 kPa for the MRE sample with $\phi = 0.118$) before the Young's modulus stops increasing. Within the non-full contact region, the MREs have poor mechanical properties. The full contact region represents the region at a suitable prestress (from 88.7 kPa to 242.6 kPa for the MRE sample with $\phi = 0.118$) where the Young's modulus and the relative MR effect roughly remain constant. The third region is the overload region which appears at large prestresses (larger than 242.6 kPa for the MRE sample with $\phi = 0.118$). Here, the zero and magneto-induced modulus decrease with increasing prestress. To further analyze the prestress-dependent mechanical properties of the MREs, a possible prestress forced deformation mechanism (figure 9) is proposed in this work. First, due to the uneven surface of the sample, only parts of the sample surface can contact the test system under small prestresses. As a result, the relevant Young's modulus is quite small and the MREs have poor mechanical properties. By increasing the prestress, the microconvexities on the sample surface are flattened, coinciding with the enlargement of the Young's modulus, ending in full contact status. Finally, due to the large prestress, the particles are forced to move toward each other, thus leading to the destruction of the internal structure of the MRE sample in the overload region. Therefore, the prestrain within the full contact region is not real deformation of the sample as a consequence of its uneven surface and needs to be modified. In the full contact region, the real prestrain ε equals the experimental prestrain ε_{exp} minus the offset prestrain $\varepsilon_{\text{offset}}$ (figure 8).

Here, the detailed mechanism of the mechanical response to prestress within the full contact region is discussed analytically. For simplicity, it is assumed that the CI particles are uniform and the spacing between adjacent particles is equivalent within the chain. When suffering from shear stress as well as being under applied prestress, the chains will deform (figure 10).

When individual particles are exposed to an applied magnetic field, they can be regarded as dipoles. The magnetic dipole moment $\vec{m}_i$ of particle i pointing along the magnetic field is given by [19]

$$\vec{m}_i = 3\mu_0\mu_{\text{m}}\beta V_{\text{p}}\vec{H}_{i\text{tot}},\ \beta = \left(\mu_{\text{p}} - \mu_{\text{m}}\right)\Big/\left(\mu_{\text{p}} + 2\mu_{\text{m}}\right) \quad (1)$$

where μ_0 is the permeability of the vacuum, μ_{m} is the relative permeability of the matrix, μ_{p} is the relative permeability of the particles, V_{p} is the volume of a single particle and $\vec{H}_{i\text{tot}}$ denotes the total magnetic field strength at particle i.

The field applied on a dipolar particle i is the result of an applied external field $\vec{H}_0$ and the local field induced by the particles around the particle i. So the magnetic field strength of particle i in a chain can be expressed as [29]

$$\vec{H}_{i\text{tot}} = \vec{H}_0 + \sum_{j\neq i}\vec{H}_j = \vec{H}_0 + 2\sum_{j=1}^{n}\frac{\left(3\hat{r}_{ij}\left(\hat{r}_{ij}\cdot\vec{m}_j\right) - \vec{m}_j\right)}{4\pi\mu_0\mu_{\text{m}}r_{ij}^3} \quad (2)$$

where $\vec{m}_j$ is the dipole moment of particle j, r_{ij} is the distance between particle i and particle j, and $\hat{r}_{ij}$ is the unit vector of $\vec{r}_{ij}$.

Here, as the MRE is macroscopically and transversely isotropic, we assume that the magnetic moments of the particles have the same magnitude and direction, i.e. $\vec{m}_i = \vec{m}_j = \vec{m}$. According to [19], when the chain-like structure (figure 10) is deformed, the magnetic field strength $\vec{H}_{\text{tot}}$ in

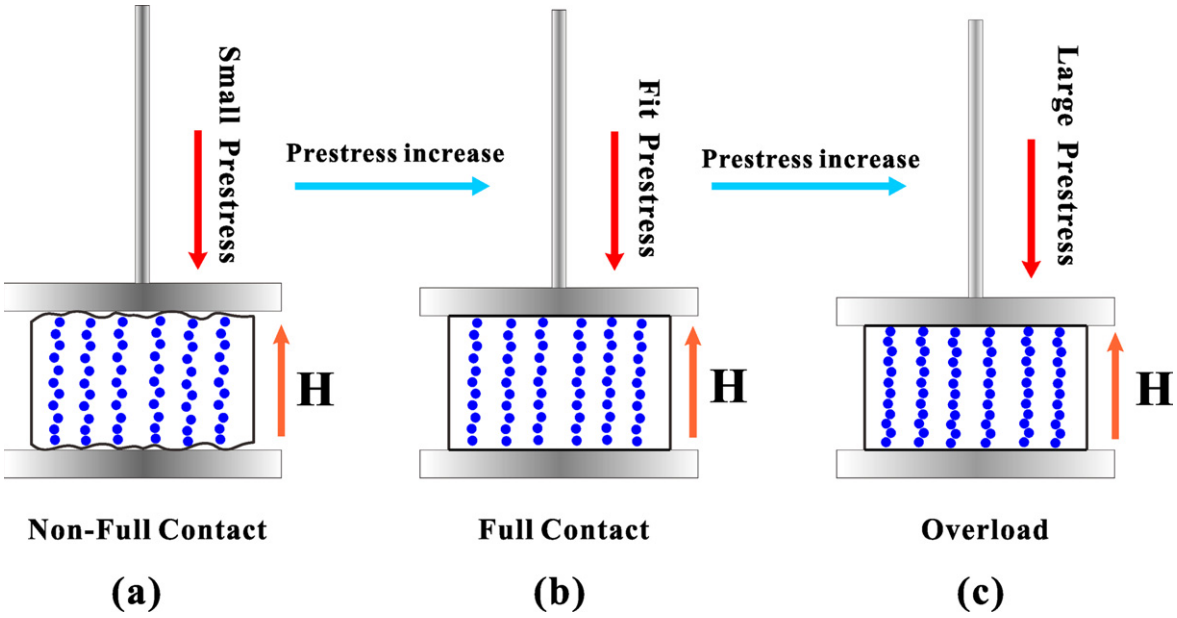

Figure 9. Mechanism of prestress forced deformation of an MRE sample at various prestresses.

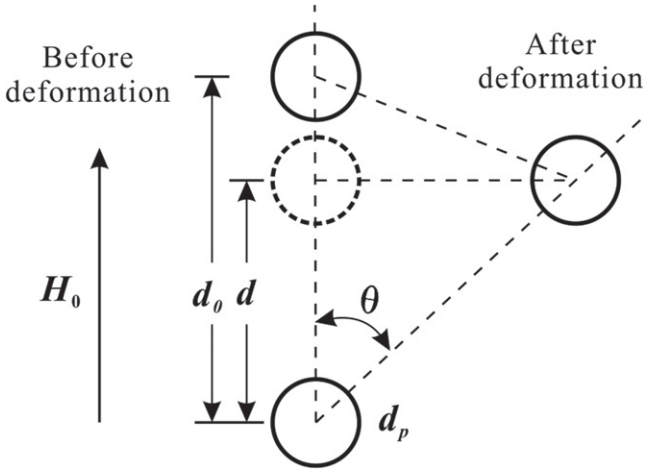

Figure 10. The deformation of particles within the chain.

the chain can be decomposed into two sectors:

$$\vec{H}_{\text{tot}} = \left(H_0 \cos\theta + \frac{Cm_{\parallel}\cos^3\theta}{\pi\mu_0\mu_{\text{m}}d^3}\right)\hat{r}_{\parallel} + \left(H_0\sin\theta - \frac{Cm_{\perp}\cos^3\theta}{2\pi\mu_0\mu_{\text{m}}d^3}\right)\hat{r}_{\perp} \tag{3}$$

where θ is the angle of the chain deformation, $C = \sum_{j=1}^{n} 1/j^3 \approx 1.202$, d is the distance between two nearby particles under prestress, $\hat{r}_{\parallel}$ and $\hat{r}_{\perp}$ are the unit vectors parallel and perpendicular to the chain, and $m_{\parallel}$ and $m_{\perp}$ are the values of the dipole moments parallel and perpendicular to the chain.

By substituting (3) in (1), we can derive

$$m_{\parallel} = \frac{\pi\mu_0\mu_{\text{m}}\beta d_p^3\cos\theta}{2 - \beta C\left(d_{\text{p}}/d\right)^3\cos^3\theta}H_0 \tag{4}$$

$$m_{\perp} = \frac{2\pi\mu_0\mu_{\text{m}}\beta d_p^3\sin\theta}{4 + \beta C\left(d_{\text{p}}/d\right)^3\cos^3\theta}H_0. \tag{5}$$

Following the classical theory of dipoles [30], the interaction energy of the two dipoles is

$$E_{12} = \frac{1}{4\pi\mu_0\mu_{\text{m}}}\left[\frac{\vec{m}_1\cdot\vec{m}_2}{r^3} - \frac{3\left(\vec{m}_1\cdot\vec{r}\right)\left(\vec{m}_2\cdot\vec{r}\right)}{r^5}\right] \tag{6}$$

where $\vec{r}$ is the distance between the two dipoles.

Thus, the interaction energy for a specific particle i in a chain can be readily obtained from (4), (5) and (6) by

$$E_i = \sum_{j\neq i}E_{ij} = 2\sum_{j=1}^{n}E_{ij} = \pi\mu_0\mu_{\text{m}}C\beta^2\left(\frac{d_{\text{p}}^6}{d^3}\right) \times H_0^2\left(\frac{2\sin^2\theta}{A^2} - \frac{\cos^2\theta}{B^2}\right)\cos^3\theta \tag{7}$$

with $A = 4 + \beta C\left(d_{\text{p}}/d\right)^3\cos^3\theta$ and $B = 2 - \beta C\left(d_{\text{p}}/d\right)^3\cos^3\theta$.

Assuming the total volume of the MRE is V, the number of particles in the matrix is

$$n = V\phi\Big/\frac{1}{6}\pi d_p^3 = \frac{6V\phi}{\pi d_p^3}. \tag{8}$$

Consequently, the total energy in the matrix is

$$E = nE_i/2. \tag{9}$$

Thus, the magnetic energy density can be obtained by

$$U = \frac{E}{V} = 3\mu_0\mu_m\phi C\beta^2 H_0^2\left(\frac{d_p}{d}\right)^3\left(\frac{2\sin^2\theta}{A^2} - \frac{\cos^2\theta}{B^2}\right)\cos^3\theta. \tag{10}$$

Moreover, as shown in figure 10, the shear strain of the chain γ and the prestrain of the sample ε, respectively, are given by

$$\gamma = \tan\theta \tag{11}$$

and

$$\varepsilon = \frac{d_0 - d}{d_0} \tag{12}$$

where d_0 is the average distance between two nearby particles within the chain in the absence of applied prestress.

Making use of (11) and (12), we obtain the magnetic energy density from (10) by

$$U = 3\mu_0\mu_m\phi C\beta^2 H_0^2\left(\frac{d_p}{d_0}\right)^3\frac{1}{(1-\varepsilon)^3} \times\left(\frac{2\gamma^2}{A_1^2} - \frac{1}{B_1^2}\right)\frac{1}{\left(1+\gamma^2\right)^{5/2}} \tag{13}$$

where $A_1 = 4 + C\beta\left(\frac{d_p}{d_0}\right)^3\frac{1}{(1-\varepsilon)^3}\frac{1}{\left(1+\gamma^2\right)^{3/2}}$ and $B_1 = 2 - C\beta\left(\frac{d_p}{d_0}\right)^3\frac{1}{(1-\varepsilon)^3}\frac{1}{\left(1+\gamma^2\right)^{3/2}}$.

The magneto-induced shear stress in the MRE can be calculated by

$$\tau = \frac{\mathrm{d}U}{\mathrm{d}\gamma}. \tag{14}$$

So the magneto-induced modulus ΔG is

$$\Delta G = \frac{1}{\gamma}\left(\frac{\mathrm{d}U}{\mathrm{d}\gamma}\right) = 3\mu_0\mu_m\phi C\beta^2 H_0^2\left(\frac{d_p}{d_0}\right)^3\frac{1}{(1-\varepsilon)^3} \cdot\left\{\frac{4-6\gamma^2}{A_1^2\left(1+\gamma^2\right)^{7/2}} + \frac{12C\beta\left(d_p/d_0\right)^3(1-\varepsilon)^{-3}\gamma^2}{A_1^3\left(1+\gamma^2\right)^{10/2}} + \frac{5}{B_1^2\left(1+\gamma^2\right)^{7/2}} + \frac{6C\beta\left(d_p/d_0\right)^3(1-\varepsilon)^{-3}}{B_1^3\left(1+\gamma^2\right)^{10/2}}\right\}. \tag{15}$$

For simplicity, we assume that the particle chains are uniformly distributed in the matrix, as shown in figure 3. Thus, the particle volume fraction of anisotropic MREs can be expressed as

$$\phi = \frac{4/3\pi\left(d_p/2\right)^3}{kd_0\cdot kd_0\cdot d_0} = \frac{\pi}{6k^2}\left(\frac{d_p}{d_0}\right)^3 \tag{16}$$

where k denotes the ratio of the average distance between two nearby single particle chains to the average distance between two nearby particles within the chain.

For the samples in the full contact region, the parameters for each sample have been calculated according to the experimental measurements and are shown in table 1.

Making use of the parameters in table 1, theoretical predictions based on (15) for MREs within the full contact region are shown in figure 11. The magneto-induced modulus non-linearly increases with increasing prestress. It is worth mentioning that the simulation results coincide well with the experimental data, especially at small volume fractions. However, due to the complexity caused by large volume fractions, the simplified model cannot perfectly match the experimental data all the time. Therefore, within the full contact region, increasing prestress can lead to an increase of prestrain and consequently cause an increase of the magneto-induced modulus. However, due to the unpredictable characteristics within the non-full contact and overload regions,

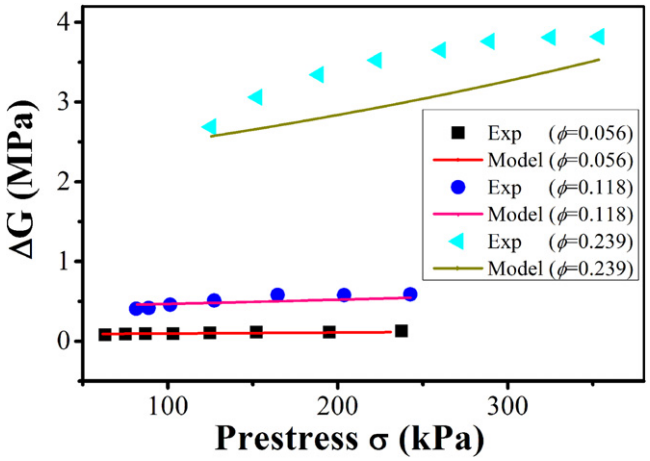

Figure 11. Comparison of the prestress between the experimental and modeling results for the magneto-induced modulus ΔG versus the applied prestress σ for different volume fraction samples.

Table 1. Values of the parameters for each sample.

Sample	γ	ε_{offset}	H_0 (kA m^{-1})	k
$\phi = 0.056$	0.005	0.0149	300	2.44
$\phi = 0.118$	0.005	0.0121	350	1.83
$\phi = 0.239$	0.005	0.0119	400	1.44

further work remains to be undertaken investigating the mechanical response of MREs at small and large prestresses.

4. Conclusions

In this work, we presented an experimental and theoretical study of the mechanical response of MREs under different prestress states. MREs with different particle volume fractions were prepared and the influence of the prestress on their dynamic properties was tested. The MREs with higher particle volume fractions exhibited better mechanical properties. With increasing prestress, both the whole storage modulus G' and magneto-induced modulus ΔG showed a declining trend after an initial ascent. Moreover, the relative MR effect remained at a high value for quite a wide fit prestress range compared to the small and large prestress. Three regions were found from the testing: the non-full contact region was due to the uneven surface of the sample, the full contact region was the suitable region in terms of practical applications and the overload region was a consequence of internal structure destruction caused by large prestresses. Finally, we proposed a model to study the mechanism of MREs within the full contact region. The theoretical analysis agreed well with the experimental results, especially at small volume fractions. This study demonstrates that the prestress can significantly affect the magneto-induced modulus by altering the spacing between particles and further dominate their practical performance in engineering applications.

Acknowledgments

Financial support from the National Natural Science Foundation of China (Grant Nos. 11372301, 11125210), Anhui Provincial Natural Science Foundation of China (1408085QA17) and the National Basic Research Program of China (973 Program, Grant No. 2012CB937500) are gratefully acknowledged. This work was supported by the Collaborative Innovation Center of Suzhou Nano Science and Technology.

References

[1] Shiga T, Okada A and Kurauchi T 1995 Magnetroviscoelastic behavior of composite gels *J. Appl. Polym. Sci.* **58** 787–92
[2] Rigbi Z and Jilken L 1983 The response of an elastomer filled with soft ferrite to mechanical and magnetic influences *J. Magn. Magn. Mater.* **37** 267–76
[3] Carlson J D and Jolly M R 2000 MR fluid, foam and elastomer devices *Mechatronics* **10** 555–69
[4] Jolly M R, Carlson J D and Munoz B C 1996 A model of the behaviour of magnetorheological materials *Smart Mater. Struct.* **5** 607–14
[5] Li W H, Zhou Y and Tian T F 2010 Viscoelastic properties of MR elastomers under harmonic loading *Rheol. Acta* **49** 733–40
[6] Li Y C, Li J C, Li W H and Du H P 2014 A state-of-the-art review on magnetorheological elastomer devices *Smart Mater. Struct.* **23** 123001
[7] Sun S S, Deng H X, Yang J, Li W H, Du H P, Alici G and Nakano M 2015 An adaptive tuned vibration absorber based on multilayered MR elastomers *Smart Mater. Struct.* **24** 045045
[8] Ginder J M, Schlotter W F and Nichols M E 2001 Magnetorheological elastomers in tunable vibration absorbers *Proc. SPIE* **4331** 103–10
[9] Yang J, Du H P, Li W H, Li Y C, Li J C, Sun S S and Deng H X 2013 Experimental study and modeling of a novel magnetorheological elastomer isolator *Smart Mater. Struct.* **22** 117001
[10] Li Y C, Li J C, Tian T F and Li W H 2013 A highly adjustable magnetorheological elastomer base isolator for applications of real-time adaptive control *Smart Mater. Struct.* **22** 095020
[11] Li Y C, Li J C, Li W H and Samali B 2013 Development and characterization of a magnetorheological elastomer based adaptive seismic isolator *Smart Mater. Struct.* **22** 035005
[12] Yang J, Sun S S, Du H P, Li W H, Alici G and Deng H X 2014 A novel magnetorheological elastomer isolator with negative changing stiffness for vibration reduction *Smart Mater. Struct.* **23** 105023
[13] Farshad M and Le Roux M 2004 A new active noise abatement barrier system *Polym. Test.* **23** 855–60
[14] Wang X, Gordaninejad F, Calgar M, Liu Y, Sutrisno J and Fuchs A 2009 Sensing behavior of magnetorheological elastomers *J. Mech. Design.* **131** 091004
[15] Galipeau E and Castañeda P P 2012 The effect of particle shape and distribution on the macroscopic behavior of magnetoelastic composites *Int. J. Solids Struct.* **49** 1–17
[16] Ju B X, Yu M, Fu J, Yang Q, Liu X Q and Zheng X 2012 A novel porous magnetorheological elastomer: preparation and evaluation *Smart Mater. Struct.* **21** 035001
[17] Mietta J L, Ruiz M M, Antonel P S, Perez O E, Butera A, Jorge G and Negri R M 2012 Anisotropic magnetoresistance and piezoresistivity in structured Fe_3O_4-silver particles in PDMS elastomers at room temperature *Langmuir* **28** 6985–96
[18] Fan Y C, Gong X L, Xuan S H, Zhang W, Zheng J and Jiang W Q 2011 Interfacial friction damping properties in magnetorheological elastomers *Smart Mater. Struct.* **20** 035007
[19] Wang Y F, He L, Yu W X and Yang X 2011 Study on the magnetorheological effect of MR elastomer under shear-compression mode *Adv. Mater. Res.* **239** 3018–23
[20] Farshad M and Benine A 2004 Magnetoactive elastomer composites *Polym. Test.* **23** 347–53
[21] Chen L, Gong X L and Li W H 2007 Microstructures and viscoelastic properties of anisotropic magnetorheological elastomers *Smart Mater. Struct.* **16** 2645–50
[22] Farshad M and Le Roux M 2005 Compression properties of magnetostrictive polymer composite gels *Polym. Test.* **24** 163–8
[23] Wang X, Gordaninejad F and Hitchcock G H 2004 Dynamic behaviors of magnetorheological fluid-elastomer composites under oscillatory compression *Proc. SPIE* **5386** 250–8
[24] Kallio M, Lindroos T, Aalto S, Järvinen E, Kärnä T and Meinander T 2007 Dynamic compression testing of a tunable spring element consisting of a magnetorheological elastomer *Smart Mater. Struct.* **16** 506–14
[25] Sun S S, Chen Y, Yang J, Tian T F, Deng H X, Li W H, Du H and Alici G 2014 The development of an adaptive tuned magnetorheological elastomer absorber working in squeeze mode *Smart Mater. Struct.* **23** 075009

[26] Danas K, Kankanala S V and Triantafyllidis N 2012 Experiments and modeling of iron-particle-filled magnetorheological elastomers *J. Mech. Phys. Solids* **60** 120–38
[27] Dong X, Ma N, Qi M, Li J, Chen R and Ou J 2012 The pressure-dependent MR effect of magnetorheological elastomers *Smart Mater. Struct.* **21** 075014
[28] Liao G J, Gong X L, Xuan S H, Guo C Y and Zong L H 2012 Magnetic-field-induced normal force of magnetorheological elastomer under compression status *Ind. Eng. Chem. Res.* **51** 3322–8
[29] Shen Y, Golnaraghi M F and Heppler G R 2004 Experimental research and modeling of magnetorheological elastomers *J. Intel. Mater. Syst. Struct.* **15** 27–35
[30] Rosensweig R E 1985 *Ferrohydrodynamics* (Cambridge: Cambridge University Press)